Faraday Discussions

Cite this: *Faraday Discuss.*, 2023, **246**, 47

PAPER

Ionic current driven by a viscosity gradient

Benjamin Wiener and Derek Stein *

Received 27th February 2023, Accepted 18th May 2023
DOI: 10.1039/d3fd00053b

Gradients of voltage, pressure, temperature, and salinity can transport objects in micro- and nanofluidic systems by well-known mechanisms. This paper explores the dynamics of particles in a viscosity gradient with numerical simulations. The different stochastic rules used to integrate the random motion of Brownian particles affect the steady-state distribution of particles in a diffusivity gradient. Importantly, the simulations illuminate the important role that the boundary conditions play, disallowing a steady-state flux when the boundary conditions mimic those of a closed container, but allowing flux when they mimic electrodes. These results provide an interpretation for measurements of a steady ionic current flowing between electrodes separated by a nanofluidic channel with a liquid viscosity gradient.

1 Introduction

Einstein famously showed that the Brownian motion of an object is fundamentally linked to its viscous drag in a fluid because the same atomic-scale bumps that cause Brownian motion also randomize the motion of a drifting particle and eventually bring it to rest.[1,2] It is not possible to know the details of the atomic-scale bumps, but one can model a Brownian motion as a string of stochastic processes that resembles a random walk.[3,4] The stochastic step size is positively related to the diffusivity, D, which is inversely related to the viscosity, η.

The mathematician Kiyosi Itô invented a method for integrating stochastic processes.[5,6] He generalized the Riemann–Stieltjes integral, whereby one divides a function into tiny intervals and sums the area under the curve based on the value of the function in each interval. A smooth function can be sampled anywhere within the interval because the possible choices all converge to the same value in the limit of small intervals. However, a Brownian motion is not smooth on any scale, and no matter how small the interval, the integral depends on the arbitrary choice of where within each interval one evaluates the function. Itô's convention is to evaluate the function at the beginning of each interval.[5]

Ruslan Stratonovich,[7,8] Donald Fisk,[9] and Peter Hänggi[10,11] later developed alternatives to Itô's integral, each giving a different but completely self-consistent formulation of stochastic calculus. The Stratonovich (–Fisk) integral evaluates the

Physics Department, Brown University, Providence, RI, USA. E-mail: derek_stein@brown.edu

function in the middle of each interval and preserves the chain rule of ordinary calculus, while the Hänggi (or isothermal) integral evaluates the function at the end of each interval.

The differences between the integration conventions are physically meaningful in the case of a Brownian particle moving in a liquid viscosity gradient because that particle's stochastic step size depends on the viscosity, and hence on its location.[12–15] Fig. 1 illustrates how the Itô, Stratonovich, and isothermal conventions affect the stochastic step size in the presence of a viscosity gradient. A particle will exhibit no average drift in a viscosity gradient if it obeys Itô's calculus, since its steps will have the same size regardless of the direction. If it evolves according to the isothermal convention, it will drift toward lower viscosity as it takes larger average steps in that direction. From another perspective, the question of integration convention boils down to how one should generalize Fick's Law of diffusion for a concentration ρ of particles, $J = -D\nabla\rho(x)$, in cases where D varies in space.[4] The Fokker–Planck generalization, which corresponds to the Itô integration rule, puts the gradient operator outside the diffusivity and gives $J = -\nabla(D(x)\rho(x))$. This results in a contribution to the flux that depends explicitly on the diffusivity gradient, the term $-\rho(x)\nabla D(x)$. The Fick generalization, which corresponds to the isothermal integration rule, leaves the gradient operator inside the diffusivity and gives $J = -D(x)\nabla\rho(x)$. This results in no explicit dependence of the flux on the diffusivity gradient.

We were inspired to explore the properties of these stochastic dynamical models in more detail when, in a series of nanofluidics experiments to be

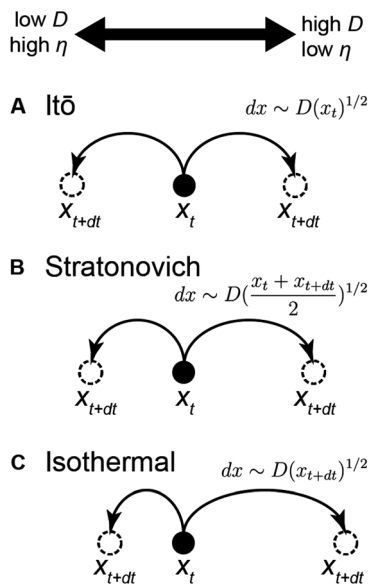

Fig. 1 Stochastic displacement models. Illustrations show leftward and rightward steps of random walks corresponding to (a) the Itô rule, (b) the Stratonovich rule, and (c) the isothermal rule. The graphic at the top indicates the directions in which the particle approaches either a region of low diffusivity and high viscosity or a region of high diffusivity and low viscosity.

reported elsewhere, we measured a current of counterions flowing in the direction of decreasing viscosity (*i.e.*, increasing diffusivity). This seemed difficult to square with the $-\rho\nabla D$ flux term in the Fick generalization (which points in the opposite direction) or the ∇D-independent flux of the Fokker–Planck generalization. It led one of us to initially believe he might have reversed the leads on the ammeter in our experiment, or in some other way inverted the current. Instead, as we will show below, it is possible to find a flux without an explicitly ∇D-dependent term in the flux expression.

The key to explaining sustained currents of the kind we measured lies in the boundary conditions. Commonly, studies of inhomogeneous diffusion focus on some closed domain which particles cannot enter or leave.[15–18] Such closed boundary conditions require a flux-less steady state.[13] On the other hand, an electrochemical system with electrodes at two or more boundaries has no such restriction. A pair of electrodes carries a faradaic current when one electrode absorbs an ion from solution, transfers the charge through an external circuit to the other electrode, which then releases another ion into solution. Periodic flux boundary conditions provide a simple model of the essential charge transfer processes at the electrodes. We show below how a viscosity gradient gives rise to a steady flux of particles inside a domain with periodic flux boundary conditions.

Along related lines, Marchesoni showed theoretically how the viscosity-induced drift of particles under the isothermal convention could be harnessed to design a Maxwell demon that transmits information in a preferred direction between boundaries that act as sources and sinks of particles.[19] Also, De Haan and Slater used simulations to show that a viscosity gradient causes a polymer, starting halfway inside a nanopore, to escape preferentially on the low-viscosity side.[20]

2 Simulation design

We studied diffusion in a viscosity gradient with a simple model for the motion of particles. The basis for our model was the work of Volpe and Wehr, which uses the stochastic differential equation,[21]

$$\mathrm{d}x_t = \sqrt{2D(x)}\,\mathrm{d}W_t \equiv \sigma(x)\,\mathrm{d}W_t, \tag{1}$$

where $\mathrm{d}x_t = x_t - x_{t'}$ is the change in position between times t and t', D is the diffusivity, $\mathrm{d}W_t = W_t - W_{t'}$ is a random variable with mean zero and variance $t - t'$. In these simulations, the continuous path of a particle is broken into discrete steps, x_n, occurring with a regular time interval Δt. It is convenient to use $\sigma(x) \equiv \sqrt{2D(x)}$, which represents the size of each random step. The discrete form of eqn (1) is

$$\Delta x = x_{n+1} - x_n = \sigma(x)\left(\pm\sqrt{\Delta t}\right). \tag{2}$$

The random variable $\mathrm{d}W_t$ in eqn (1) has been represented in eqn (2) by a discrete random variable $\pm\sqrt{\Delta t}$ (where the $\pm$ represents the random choice), which has variance Δt. We set $\Delta t = 1$ and used a spatial domain 100 units wide. Typically, in simulations like this one, when a particle would pass through a boundary at $x = 0$ or $x = 100$, it is instead reflected back into the domain.[21] Fig. 3a shows a diagram of a particle whose final position would have sent it past the boundary by

a distance a. Instead, the particle is placed a distance a inside the domain. This rule is known as a reflective boundary condition.[21]

For a system without a diffusivity gradient, the application of eqn (2) is uncomplicated. We simply generate a random choice, either $\sqrt{\Delta t}$ or $-\sqrt{\Delta t}$, multiply it by σ, add the result to x_n, and repeat. Fig. 2a shows five sample trajectories for particles with $D = 1$. Particles are just as likely to go in either direction. The particles start tightly clustered but spread out over time. By 1000 steps, they look randomly distributed. The purple trajectory in Fig. 2a shows a particle bumping against the wall at $x = 100$. Fig. 2b shows the distributions of 10^5 particles with uniform diffusivity $D = 1$ after 10, 100, and 1000 time steps. The particles were released from an initially Gaussian distribution centered at $x = 50$ with a standard deviation 1. The sharply peaked distribution spreads symmetrically about $x = 50$, relaxing to a half-max width of about 10 after 10 time steps and 35 after 100 steps. By step 1000, the distribution was nearly flat. We compared the simulated distributions with the analytic solution for point-source free diffusion: a Gaussian function whose width increases with time,

$$\rho(x,t) = \frac{N}{\sqrt{4\pi Dt}} e^{-x^2/4Dt}, \tag{3}$$

where N is the number of particles. Our simulation matches eqn (3) well after 10 and 100 steps, but shows an overabundance of particles everywhere after 1000 steps. This is because eqn (3) is a solution for diffusion in free space, but our simulation will not let particles leave the domain.

Introducing a diffusivity gradient complicates the model in an important way. Each particle begins a step at a position x_n and ends at x_{n+1} so we have to choose where in that interval to evaluate function $\sigma(x)$; any location from x_n to x_{n+1} is equally valid. We could use the Itô convention, evaluating the diffusivity at the beginning of the step:

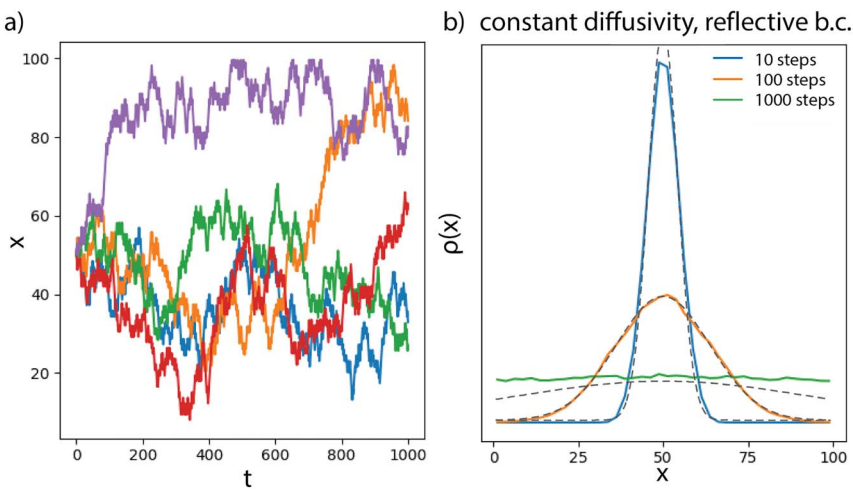

Fig. 2 Simulated diffusion of 10^5 particles with reflective boundary conditions and spatially-constant diffusivity. (a) Five sample particle trajectories. (b) The distribution of particles after 10, 100, and 1000 time steps. Dashed lines show theoretical expectation according to eqn (3).

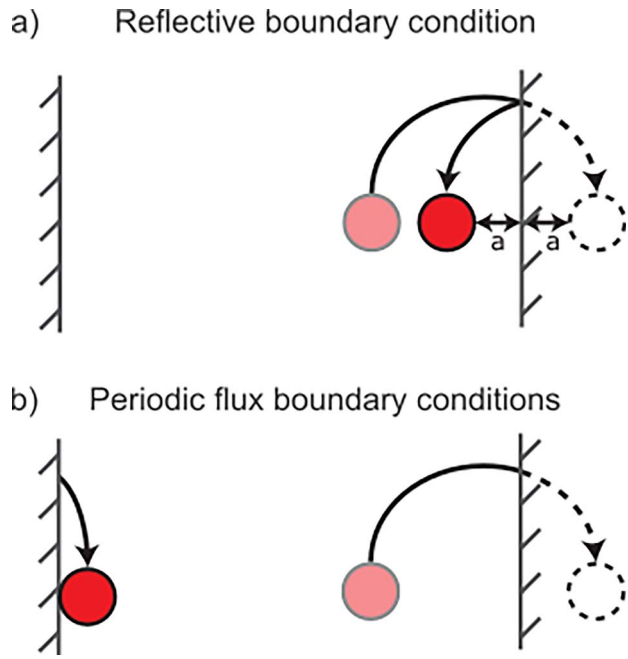

Fig. 3 (a) A particle hopping into a reflective boundary condition. (b) A particle encountering periodic flux boundary conditions that serve as a simple model of electrodes.

$$x_{n+1} = x_n \pm \sigma(x_n)\sqrt{\Delta t}. \tag{4}$$

We could use the Stratonovich convention, evaluating the diffusivity in the middle of the step:

$$x_{n+1} = x_n \pm \sigma\left(\frac{x_{n+1} + x_n}{2}\right)\sqrt{\Delta t}. \tag{5}$$

Finally, we could use the isothermal convention, evaluating it at the end:

$$x_{n+1} = x_n \pm \sigma(x_{n+1})\sqrt{\Delta t}. \tag{6}$$

The Itô convention, represented by eqn (4), is the easiest to implement in a simulation because we know the current position of each particle and can straightforwardly compute the value of $\sigma(x_n)$. Eqn (5) and (6) present an apparent catch-22. They require us to know where the particle will land to find the step size, but, of course, we must know the step size to compute where the particle will land. We will show how to find x_{n+1} in a self-consistent manner by first noting that eqn (4)–(6) can be expressed as special cases of a more general equation in which a continuous parameter α represents the choice of where to evaluate $\sigma(x)$,

$$x_{n+1} = x_n \pm \sigma(x_n + \alpha\Delta x)\sqrt{\Delta t}. \tag{7}$$

The parameter α runs from 0 to 1, and eqn (4)–(6) are special cases with $\alpha = 0$, 1/2, and 1 respectively. We Taylor expand eqn (7) to first order about the point x_n to find an equation for x_{n+1} based on x_n and the gradient in the diffusivity,

$$\sigma(x_n + \alpha\Delta x) \approx \sigma(x_n) + \alpha\frac{\mathrm{d}\sigma(x)}{\mathrm{d}x}\Delta x. \tag{8}$$

Substituting in eqn (2) gives

$$\sigma(x_n + \alpha\Delta x) \approx \sigma(x_n) \pm \alpha\sigma(x_n)\frac{\mathrm{d}\sigma(x_n)}{\mathrm{d}x}\sqrt{\Delta t} \tag{9}$$

and applying to eqn (7) gives a way to calculate x_{n+1} in terms of x_n for any value of α,

$$x_{n+1} = x_n + \alpha\sigma(x_n)\frac{\mathrm{d}\sigma(x_n)}{\mathrm{d}x}\delta t \pm \sigma(x_n)\sqrt{\delta t}. \tag{10}$$

In terms of $D(x)$, this would be,

$$x_{n+1} = x_n + \alpha\frac{\mathrm{d}D(x_n)}{\mathrm{d}x}\delta t \pm \sqrt{2D(x_n)\delta t}. \tag{11}$$

Consider a step subject to the isothermal rule as given by eqn (7) with $\alpha = 1$. The diffusive third term in eqn (7) updates the position based on $\sigma(x_n)$, as prescribed by the Itô convention. By adding the second term, sometimes called the spurious or noise-induced drift, we recover the results of the isothermal convention.[4,21,22] In other words, a trajectory in the isothermal convention is equivalent to one in the Itô convention with an added drift term.[21,22]

3 Results of simulations with diffusivity gradients

3.1 Using reflective boundary conditions

In their paper, Volpe and Wehr studied the Itô, Stratonovich, and isothermal integration conventions using simulations and demonstrated how this choice affects the steady-state particle distribution, finding a monotonically decreasing particle density when using the Itô convention, and a flat one when using the isothermal convention.[21] We set our simulation parameters to match those of Volpe and Wehr's, including $\sigma(x) = 0.2 + 0.02x$, a formula estimated from Fig. 4 of ref. 21. Importantly, we used the same reflective boundary condition shown in Fig. 3 that Volpe and Wehr did. The simulation contains 10^5 particles with an initial Gaussian distribution with mean 50 and standard deviation 1, sampled at intervals up to 10^6 time steps, enough to reach the steady state.

Our results closely match those of Volpe and Wehr. Fig. 4a shows the distribution of particles in a simulation of diffusion using the Itô convention. After 10 and 100 steps, the initial distributions widened and skewed slightly to the left. By $t = 10^3$, the tails of the distribution reached the boundaries, and the distribution is skewed noticeably left. It is clear the system has reached steady state by 10^4 steps because no further change is visible by 10^5 steps. Particles have piled up against the left boundary. After reaching the steady state, we measured no significant flux across $x = 50$.

Likewise, Fig. 4b shows diffusion under the $\alpha = 1$ or isothermal convention. The distributions look roughly Gaussian until 10^2 steps. After 10^3 steps, the distribution has reached the boundary at $x = 100$, but not the one at $x = 0$. By 10^4 steps, the system reached a steady state with a flat distribution and no significant flux through $x = 50$.

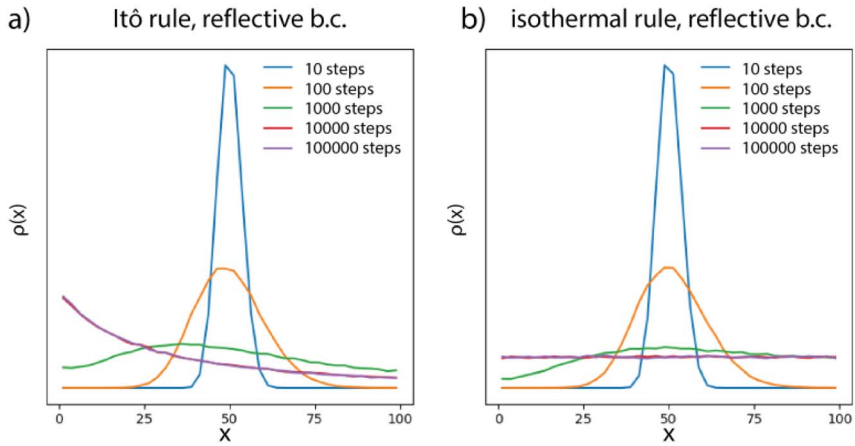

Fig. 4 Simulated diffusion of 10^5 particles with reflective boundary conditions using different integration conventions. Evolution of the particle distribution using (a) the Itô convention and (b) the isothermal convention.

The absence of flux in these cases is not a surprise. In a closed container like the one simulated here, flux cannot exist anywhere in steady state. This constraint, along with spatial differences in hop length, allows us to understand the asymmetric steady state distribution resulting from the Itô rule in Fig. 4a, as well as the flat distribution resulting from the isothermal rule in Fig. 4b. Fig. 5a shows, for an arbitrary test point x', the farthest points to the left and right from which particles are capable of hopping to or past x' for the Itô convention. The region on the right is always larger than that on the left because the diffusivity increases toward the right so hops originating from that direction are longer. Fig. 5a also shows the equilibrium particle distribution, as calculated by our simulation and shown in Fig. 4a. The regions under the ρ curve shaded with orange and blue and are proportional to the number of particles that can possibly pass x' from the left and right respectively. Since particles jump left and right with equal probabilities in our model, the areas of these regions are proportional to the average number of particles that will cross x' in each direction in a given time step. Any difference in these areas indicates that a net flux will flow away from the larger region. The system must reach an equilibrium where the particle distribution always decreases toward the right in a way that compensates for the difference in hop length and brings the shaded areas into equality.

Fig. 5b again shows the region to the left and right of an arbitrary point x' inside which particles are capable of hopping past x', but this time for the isothermal rule. The hop lengths are based on the hop's end position, so the sizes of these regions are equal. In this closed system, the flux must eventually reach zero everywhere. For the shaded regions to be equal for every choice of x', the equilibrium distribution must be flat, which is what we see in Fig. 4b. Eqn (10) suggests another perspective from which to view the isothermal convention of stochastic motion. As hopping with hop-length determined by the starting position, with a superimposed drift proportional to the gradient in the diffusivity.

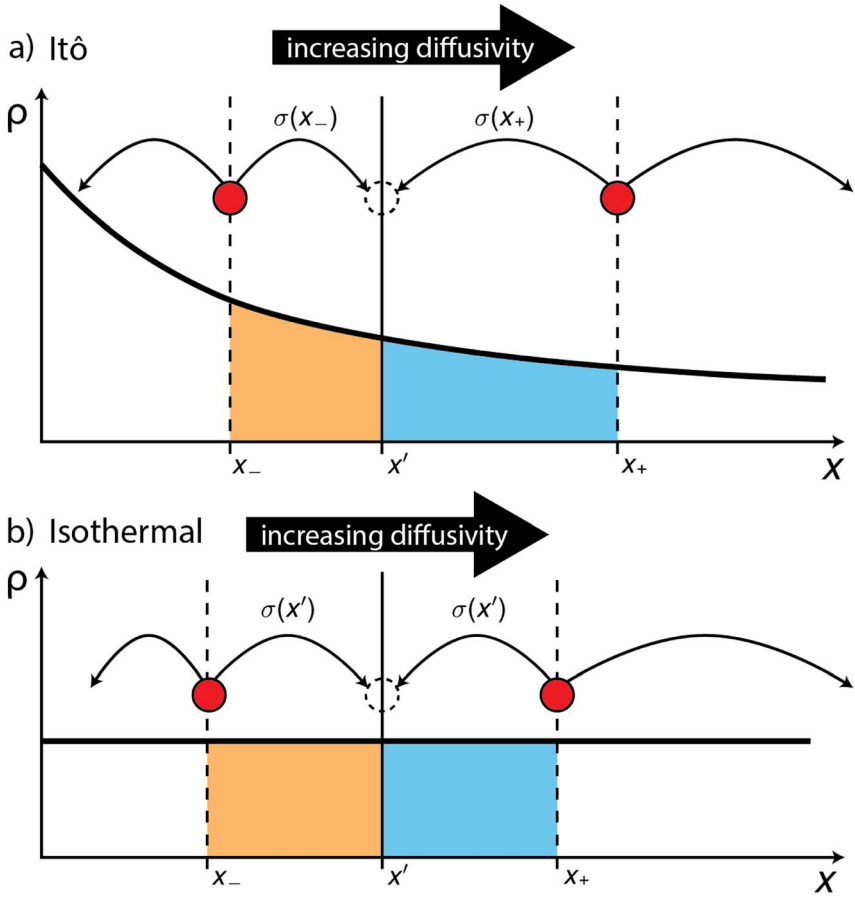

Fig. 5 Simulated equilibrium particle densities in the (a) Itô convention and (b) isothermal convention. Dotted lines show the farthest positions, x_+ and x_-, from which particles can cross a test point, x', from the left and right respectively. The areas of the shaded regions below the curve are proportional to the approximate number of particles that can cross x' from the left (orange) and the right (blue) in one step.

Which stochastic integration convention gives the correct physical description of ions in a liquid? The isothermal convention is strongly preferred on thermodynamic grounds: only the isothermal convention gives a uniform particle distribution in a closed domain at thermal equilibrium, so it alone respects the Boltzmann distribution.[13]

3.2 Using periodic flux boundary conditions

The reflective boundary conditions used above are a poor model of experiments involving electrodes that can carry faradaic currents. When an ion arrives at an electrode, it can initiate a string of processes that result in a net transfer of one ion to a distant location: the electrode absorbs the ion and quickly transfers the charge through an external circuit to a second electrode, which releases a new ion into solution. This sequence preserves the charge neutrality of the liquid and

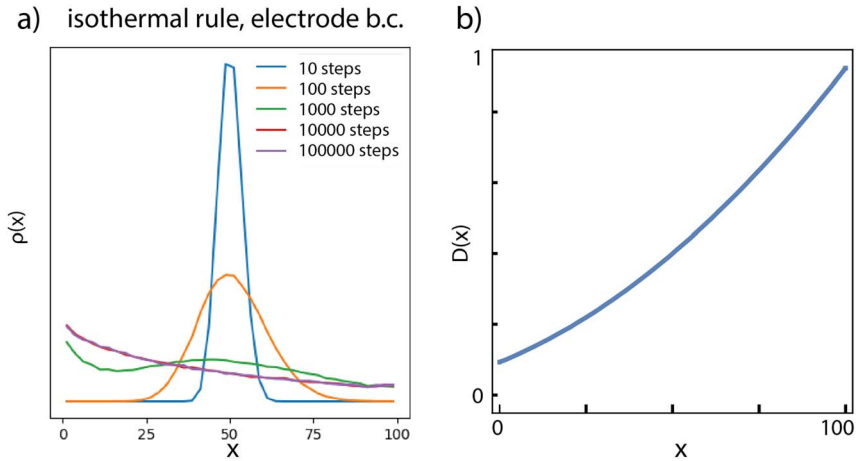

Fig. 6 Simulated diffusion of 10^5 particles with periodic flux boundary conditions using the isothermal convention. (a) Evolution of the particle distribution. (b) Diffusivity as a function of x.

breaks the requirement that the flux between the electrodes be zero. Imposing periodic flux boundary conditions at electrode surfaces offers a simple way to model the essential behavior. We imposed periodic flux boundary conditions in our one-dimensional particle simulations as follows: any particle that would pass a boundary in the simulation is counted and moved to the opposite boundary. Fig. 3b illustrates a particle hopping into the right boundary and inducing a new particle to be released into the domain from the opposite boundary.

Fig. 6a shows the evolution of the simulated particles distribution using the isothermal convention. This simulation was the same as the one in Fig. 4b, but with the periodic flux boundary conditions described above. Fig. 6b shows the diffusivity function used in the simulation. By step 10^4, the system reached the steady state. This time, the distribution is not flat. The concentration is highest on the left and decreases monotonically to the right.

Fig. 7a illustrates the regions in which particles can reach or pass x' in one step, along with the distribution of particles found in the isothermal experiment with periodic flux boundary conditions. The left shaded region under the curve is larger than the right shaded region, meaning that we expect net right-ward flux. In the steady state, this flux must be constant for every choice of x', including at the boundaries. This constraint determines the magnitude of the flux. Fig. 7b shows the regions inside which particles can reach the boundaries at $L = 0$ and $L = 100$. The difference in the areas of these regions represents the flux through the boundary, which must be equal to the flux everywhere else in the steady state.

4 Comparison with experiment

Our simulations show the effects of the integration convention and boundary conditions, but do they predict currents that are measurable in experiments? We performed simulations that approximate the features of experiments in which we varied the liquid viscosity at both ends of a nanochannel. The channel length L

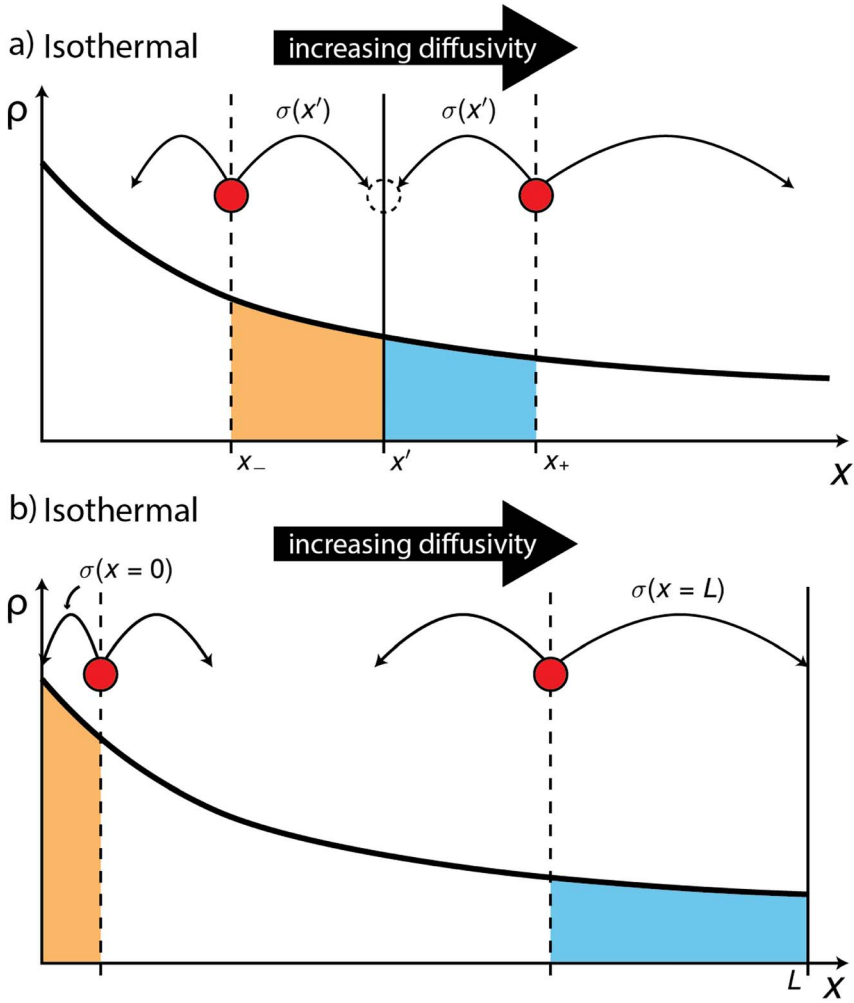

Fig. 7 Simulated equilibrium particle density in the isothermal convention with periodic flux boundary conditions. (a) Dotted lines show farthest positions from which particles can reach or cross a test point, x', from the left and right. The areas of the shaded regions are proportional to the number of particles that can reach or cross x' from the left (orange) or right (blue) in one step. (b) Dotted lines show the farthest positions from which particles can reach or cross the boundaries at $L = 0$ and $L = 100$. Area of the shaded regions is proportional to the number of particles with a chance to hit the boundary at $x = 0$ (orange) or $x = 100$ (blue) in one step.

could vary from 50 to 200 in units of micrometers. In the simulations discussed above, we used linear functions for $\sigma(x)$ to match the conditions used by Volpe and Wehr.[21] In the simulations reported below, we used a linear diffusivity gradient to describe the inside of the nanochannel, where two different liquids would intermix. We used a flat initial particle distribution to hasten the arrival at the steady state. We modeled the particle dynamics using the isothermal integration rule, and we modeled the electrodes by imposing periodic flux boundary conditions.

The result, we noticed, was that the simulator would initially register flux at the boundaries, but no flux at the center. After a relatively long delay, the flux at the center would catch up. Fig. 8a shows the evolution of a flat particle distribution toward the steady state. The initially flat distribution at the midpoint of the channel explains the lack of flux there. The gradient in $\rho(x)$ seems to build in from the boundaries. Fig. 8b shows the absolute difference between the center and boundary fluxes (as a fraction of the boundary flux) for a range of times as the system approaches the steady state. Two different simulations, with domain sizes of 100 and 200, are compared. Initially, the fractional flux difference is 1, because all of the flux is at the boundary. At about step 2000 for the $L = 100$ simulation and step 10 000 for the $L = 200$ simulation, that difference starts to drop. Eventually, the difference becomes negligible as the fluxes converge to the same number and the system enters the steady state. We used analysis like this to guide the lengths of our simulations.

To compare with our viscosity-varying experiments, we performed simulations with a variety of diffusivity profiles. We simulated 10^5 particles according to the isothermal rule for 2×10^5 time steps, counting flux for the last 5×10^4 steps. After the system reached equilibrium, we started counting the flux at the boundaries and at $x = L/2$.

Fig. 9 shows the simulated flux as a function of the viscosity at the right end of the domain, $\eta(x = 100)$, with the viscosity at the left end held constant at $\eta(x = 0) = 10$. The inset shows the diffusivity profiles corresponding to each data point. We have used the viscosity at the right end as the independent variable because it is relatively straightforward to control that parameter in an experiment. The interpretation of the results is clear: particles flow toward lower viscosity. When the viscosity is lower at the right end than the left, the flux of particles is positive (rightward). When the viscosity is higher at the right than the left, the flux of particles is negative (leftward). We also note that the curve flattens out as the right viscosity increases. This can be understood as a slowing of the transport processes as the average viscosity in the channel increases.

Fig. 10a shows the simulated flux as a function of the simulation domain size. The particle number density, N/L, and diffusivities at the boundaries, $D(x = 0)$ and $D(x = L)$, were kept constant. Fig. 10b shows the diffusivity gradients used, where

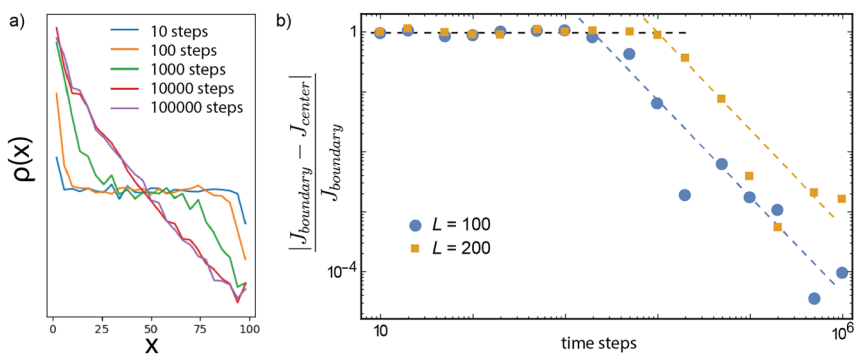

Fig. 8 (a) The evolution of an initially flat particle distribution with the isothermal rule and electrode boundary conditions. (b) The fractional absolute difference in flux at the center and at the boundaries for simulations with domain sizes of 100 and 200.

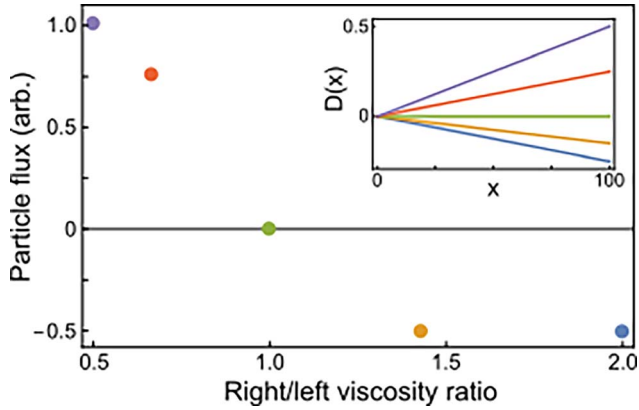

Fig. 9 Simulated particle flux obtained using the isothermal rule and periodic flux boundary conditions for several values of the viscosity at the right end of the channel relative to the fixed viscosity at the left end. Inset shows the diffusivity profiles, with colors corresponding to the symbols in the main plot.

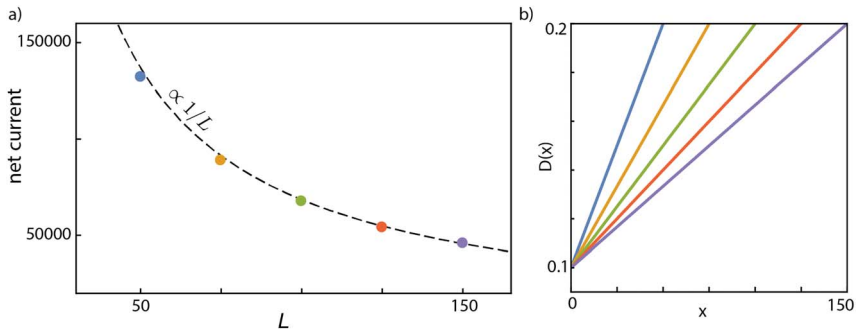

Fig. 10 Simulated flux in simulations with several domain lengths using the isothermal rule and periodic flux boundary conditions. (a) Dependence of flux on L. The flux is measured in simulation units corresponding to net crossings of the right boundary in the final 5×10^4 time steps of each simulation. (b) Diffusivity profiles, color coded to match points in (a).

the color corresponds to the color of the data points in Fig. 10a. As the domain gets longer, the gradient decreases and so does the drift speed. The dotted line in Fig. 10a shows the expected flux dependence, $1/L$. This matches the linear dependence of the current on the viscosity gradient observed experimentally.

5 Conclusions

Simulations have illuminated the mechanisms of diffusive ion transport in a gradient of liquid viscosity. The boundary conditions turn out to be essential. The reflective boundary conditions that simulate a closed container make it impossible for a steady-state flux to exist. However, boundary conditions which model the ability of electrodes to absorb and release ions at different locations allow a steady-state flux. Using the isothermal convention and periodic flux boundary conditions,

particles exhibit a noise-induced drift in the direction of lower viscosity that produces a flux, and this flux has the important features of ionic currents measured in our nanochannels. Finally, we note that a viscosity-driven current of particles does not violate any thermodynamic principle. In order to experimentally maintain a viscosity gradient in a nanochannel, one needs to replenish the different-viscosity liquids at either end, and this holds the system out of equilibrium. As the liquids intermix, the free energy of mixing is available to drive a steady current.

Conflicts of interest

There are no conflicts of interest to declare.

Acknowledgements

This material is based upon work supported by the National Science Foundation under Grant No. 1904511 and by Oxford Nanopore Technologies, Ltd.

Notes and references

1 A. Einstein, *Ann. Phys.*, 1905, **322**, 549–560.
2 M. Von Smoluchowski, *Ann. Phys.*, 1906, **326**, 756–780.
3 S. Chandrasekhar, *Rev. Mod. Phys.*, 1943, **15**, 1.
4 N. G. Van Kampen and W. P. Reinhardt, *Stochastic Processes in Physics and Chemistry*, 1983.
5 K. Itô, *Proc. Imper. Acad.*, 1944, **20**, 519–524.
6 R. Jarrow, P. Protter et al., in *A Festschrift for Herman Rubin*, Institute of Mathematical Statistics, 2004, pp. 75–91.
7 R. Stratonovich, *Vestn. Mosk. Univ. Seriya 1 Mat. Mekhanika*, 1964, **1**, 3–12.
8 R. Stratonovich, *SIAM J. Control*, 1966, **4**, 362–371.
9 D. L. Fisk, *Quasi-Martingales and Stochastic Integrals, Michigan State Univ East Lansing Technical Report*, 1963.
10 P. Hanggi, *Helv. Phys. Acta*, 1980, **53**, 491–496.
11 P. Hänggi and H. Thomas, *Phys. Rep.*, 1982, **88**, 207–319.
12 N. Van Kampen, *J. Phys. Chem. Solids*, 1988, **49**, 673–677.
13 A. W. Lau and T. C. Lubensky, *Phys. Rev. E*, 2007, **76**, 011123.
14 I. Sokolov, *Chem. Phys.*, 2010, **375**, 359–363.
15 G. Volpe, L. Helden, T. Brettschneider, J. Wehr and C. Bechinger, *Phys. Rev. Lett.*, 2010, **104**, 170602.
16 E. R. Dufresne, D. Altman and D. G. Grier, *Europhys. Lett.*, 2001, **53**, 264.
17 J. Happel and H. Brenner, *Low Reynolds Number Hydrodynamics: With Special Applications to Particulate Media*, Springer Science & Business Media, 2012, vol. 1.
18 E. Kätelhön, S. V. Sokolov and R. G. Compton, *Sens. Actuators, B*, 2016, **234**, 420–425.
19 F. Marchesoni, *Materials*, 2013, **6**, 3598–3609.
20 H. W. de Haan and G. W. Slater, *Phys. Rev. E*, 2013, **87**, 042604.
21 G. Volpe and J. Wehr, *Rep. Prog. Phys.*, 2016, **79**, 053901.
22 H. W. de Haan, M. V. Chubynsky and G. W. Slater, *arXiv*, 2012, preprint, arXiv:1208.5081, DOI: **10.48550/arXiv.1208.5081**.